A high throughput spectral image microscopy system

M. Gesley, and R. Puri

Citation: Review of Scientific Instruments **89**, 013705 (2018); doi: 10.1063/1.4998725
View online: https://doi.org/10.1063/1.4998725
View Table of Contents: http://aip.scitation.org/toc/rsi/89/1
Published by the American Institute of Physics

A high throughput spectral image microscopy system

M. Gesley[a] and R. Puri
Spynsite LLC, 31 Rydal Court, Oakland, California 94611, USA

(Received 2 August 2017; accepted 18 December 2017; published online 22 January 2018)

A high throughput spectral image microscopy system is configured for rapid detection of rare cells in large populations. To overcome flow cytometry rates and use of fluorophore tags, a system architecture integrates sample mechanical handling, signal processors, and optics in a non-confocal version of light absorption and scattering spectroscopic microscopy. Spectral images with native contrast do not require the use of exogeneous stain to render cells with submicron resolution. Structure may be characterized without restriction to cell clusters of differentiation. *Published by AIP Publishing.*
https://doi.org/10.1063/1.4998725

I. INTRODUCTION

The ability to rapidly measure large microscopic distributions is of interest in fields including medicine, biotechnology, and materials science. Flow cytometry has proven an invaluable tool for studying cell populations.[1] The number of illumination and detection wavelengths has been extended over time and coupled with an increased range of fluorophores attached via monoclonal antibodies to clusters of differentiation on cell surfaces and in some cases to intracellular entities.[2] However, robust detection of large cell populations remains a challenge for clinical use. It is technically possible to achieve 20 000 (events/s) flow rates;[3] however, a 1% measuring precision constrains rates to <10 000 cells/s with a detection limit of a few hundred fluorescent molecules per cell.[4] Rates are limited, in part, by cell fragility or fluidics delivery, which presents a stream of cells in a serial manner for detection. Flow cytometers have accurately examined cells up to 7000 (cells/s);[5] in this case, sorting 5×10^9 total cells to find 5 rare cells requires 200 (h). Thus, rare cell detection at part per billion accuracies in less than one day remains a problem. Advanced methods to identify rare cells in the blood may improve diagnostic capabilities and medical outcomes for patients with invasive medical procedures replaced by peripheral blood tests. Improved detection of immunofluorescent labeled rare cells can be achieved by increasing the field of view (FOV) using a fiber-optic array scanning technology.[6] Confocal Raman microscopy is a method for reagent-less identification of various bio-entities at high resolution[7] but requires long exposure times to compensate for small scattering cross sections. Spectral image comparison can be used to differentiate cancer cells from normal lymphocytes.[8–10] Confocal light absorption and scattering spectroscopy (CLASS) has been introduced as a method for observing sub-micrometer intracellular structures in living cells that do not require exogeneous labels.[11] The CLASS method was first applied to noninvasive detection and differentiation of adult and fetal nucleated red blood cells (fNRBC), which make up a small fraction $1{:}10^9$ of circulating cells during pregnancy where a 1 (ml) sample may capture a few fNRBC.[12] The CLASS results were obtained without cell damage or use of fluorophores but did not describe how to achieve high throughput.

The present work describes a high throughput spectral imaging microscopy system capable of rare cell detection in a few hours. To overcome flow cytometry rate limits and use of fluorophore tags, a system architecture integrates sample mechanical handling, signal processors, and an optics, which permits native contrast imaging via a non-confocal extension of light absorption and scattering spectroscopic microscopy.

II. HIGH THROUGHPUT SPECTRAL IMAGE MICROSCOPY

To rapidly measure large cell populations, the spectral imaging microscopy system (a) shown in Fig. 1 balances performance among three subsystems:[13] sample-stage mechanical motion (b), an optics—shown in a reflection configuration (c), and a compute platform. The pixel array sensor, analog to digital electronics (d), and data link (e) transmit frames to the host computer (f) and storage device (g). Stage and camera control is coordinated with signal processing and spectral object rendering and classification.

A. Spectral imaging optics

A broadband source coupled with a tunable filter generates a sequential set of narrow bands to illuminate a sample, Fig. 2. Broad area Kohler illumination[14] supports high throughput parallel pixel exposure and reduces light flux to avoid cell damage with visible light wavelengths $\lambda \sim 440$ nm–650 nm. The absence or presence of a beam block produces bright- or dark-field imaging, respectively.

A reflective optics can also sequentially illuminate a sample field of view (a) with uniform illumination (b) (solid lines) over a range of wavelengths generated by a broadband visible light source (c) and tunable filter (i), Fig. 3. A supercontinuum laser produces picosecond pulses over a wide range of frequencies in the visible spectrum with high spectral density.[15] A 6W source (Fianium SC450-6) generates a 500-700 nm spectral bandwidth from a 100 (ps) master pulse having a 1 (MHz) repetition rate with a spectral density of 3 (nJ/nm),

[a]Electronic mail: gesley@spynsite.com.

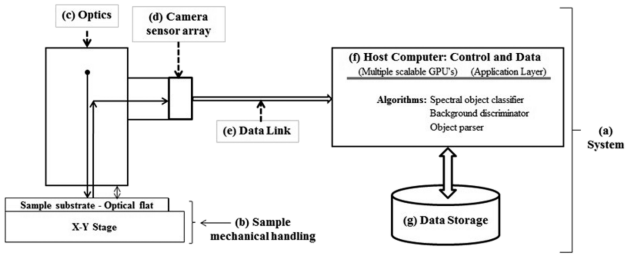

FIG. 1. Schematic of a high throughput spectral microscopy system.

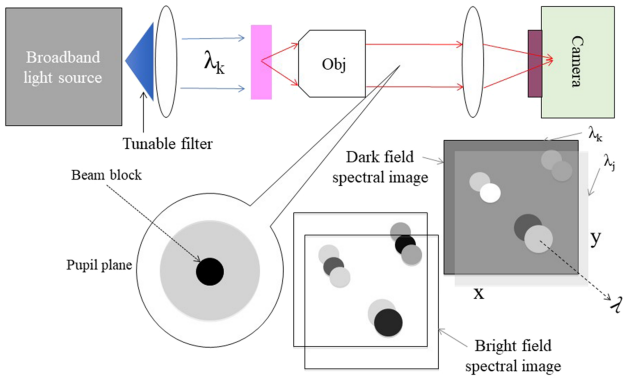

FIG. 2. Spectral imaging concept with a transmission optic.

which results in a randomly polarized light power output of 3 (mW/nm). An acousto-optic tunable filter (AOTF) (i) assumed operating at approximately 100% efficiency passes $\Delta\lambda = 20$ nm with 60 (mW/band) transmitted in ~25 (μs). Transmission efficiency of ~50% occurs from randomly polarized laser emission and linearly polarized light passed by the tunable filter. A polarizing beam splitter (k) separates illumination from collection. Given s-polarized light is transmitted out of a tuned filter, a range of p-polarized light dispersed from a sample field of view (a) arrives at the pixel sensor array. If 10% of s-polarized light is transmitted to a sample with p-polarized light reflected by a beam splitter, then 3.0 (mW) may be received by the sensor. Polarization rotation may improve transmitted power as a polarizing beam-splitter typically transmits p-polarized light and reflects s-polarized light more efficiently.

A transmission optic may be used [Fig. 4 (left)] that retains the supercontinuum laser and doubles transmission efficiency by omitting a beam splitter. As a result, the photoelectron current density generated by the CCD from the illuminated sample should be approximately the same as achieved in the reflection mode. A prototype used to produce example spectral images is shown in Fig. 4 (right) comprising a xenon arc lamp, a monochromator, a CCD camera, a 10× objective with numerical aperture (NA) = 0.5, and a 1.8× zoom lens. A 0.4 (μm) diameter sample-object is transferred to a 6.45 (μm) CCD-pixel at the sensor with 18× magnification. Magnification is calibrated with a 5.0 μm grating and 0.5 μm diameter polystyrene beads.

Chromatic distortion degrades spectral maps by adding extra positional shifts to geometric distortions of a field of view (FOV) over measured wavelengths. Well-corrected optics can minimize chromatic distortion; however, residual errors may be further reduced by adjusting frame pixel coordinates based on calibration measurements. As wavelength changes, a relatively small and high contrast calibration site may present variable contrast among neighboring pixels. Figure 5 (left) shows a white-dashed 4 × 2 pixel rectangle calibration reference enclosing eight pixels whose intensities vary over the wavelength series. Error vectors of 2.4 to 3.8 μm magnitude are shown on a magnified scale in Fig. 5 (right). A nonlinear chromatic distortion across a FOV may be compensated by calibrations at multiple sites with an interpolating distortion lookup table if required.

B. Signal processing

Source brightness and optics determine photons/area that illuminate a sample surface. Sample characteristics, transmission efficiency, and magnification also influence the signal generated by a sensor array (3e) comprised of a charge coupled device (CCD) or a complementary metal-oxide-semiconductor (CMOS) and delivered in the frame image output (3h). A sensor illumination of 3.0 (mW)/4 × 10^{-19} (J) = 7.5 × 10^{15} (photons/s) using λ = 500 (nm), energy 2.5 eV = 4 × 10^{-19} (J), and 50% quantum efficiency over the 450-750 (nm) visible range yields 3.8 × 10^{15} (electrons/s). A signal to noise estimate is determined for a 1.43 (Mpixel) CCD (Sony ICX285) with full well (1 × 1 binning) = 1.8 × 10^4 (electrons), 30 MHz read rate noise = 12.3 (electrons/pixel), and dark

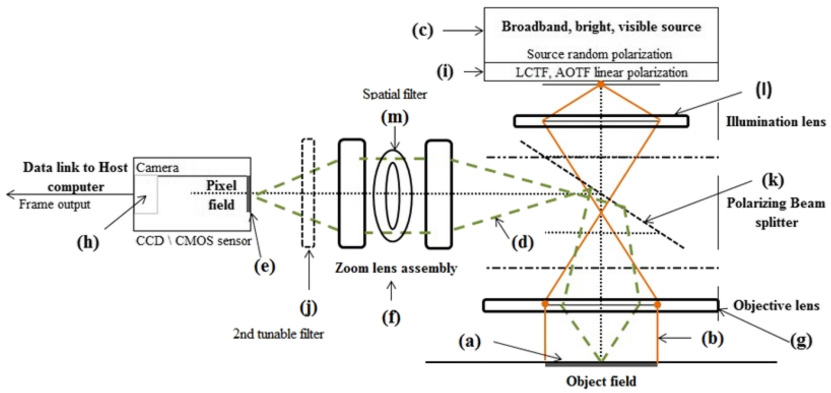

FIG. 3. The figure is a schematic diagram showing a reflective optics.

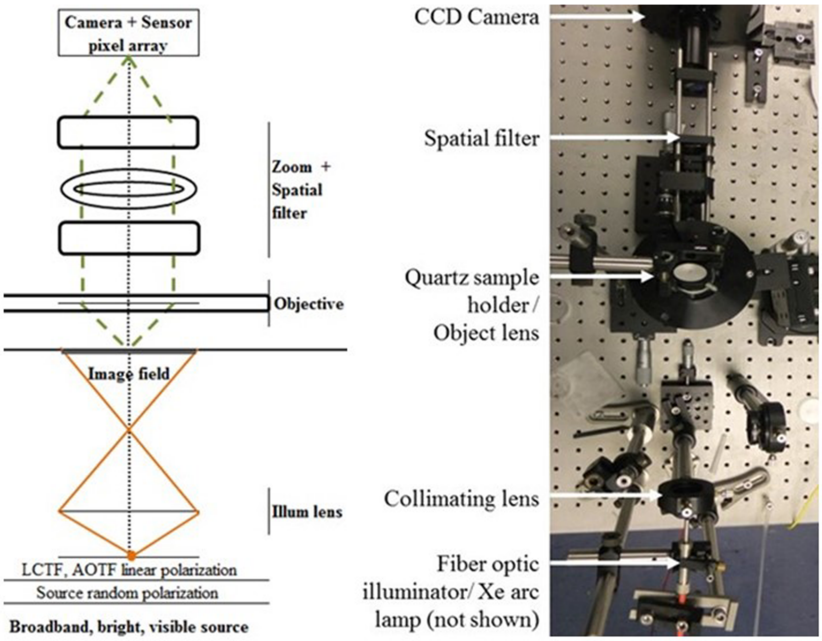

FIG. 4. (left) a transmission optic schematic; (right) a benchtop configuration (Courtesy of UC Davis Center for Biophotonics).

current = 1.5 x 10^{-2} [electron/(s/pixel)]. The dynamic range $= {Full\ well}/{Read\ noise} = 1463$ effectively delivers an 11-bit gray pixel, less than a specified 14 bits. A photoelectron current density 3.8×10^{15} (electrons/s)/1.43 (Mpixels) = 2.62×10^{9} [electrons/(s/pixel)] = 4.2×10^{-10} (A/pixel) generates a signal $S = 2.62{\times}10^{9}\left({e^{-}}/{s \times pixel}\right){\cdot}3.3{\times}10^{-8}$ (ms) = $87\left({e^{-}}/{pixel}\right)$ at a 30 MHz read (CCD refresh) rate. The signal to noise (S/N) is primarily determined by read noise ${S}/{N_{read}} = \frac{87}{12.3} = 7.1$ as the dark noise level $N_{dark\ noise} = 1.5{\times}10^{-2}\left({e^{-}}/{s \times pixel}\right) \cdot 33.3\ (\text{ms}) = 5 \times 10^{-3}\left({e^{-}}/{pixel}\right)$ is negligible at a 30 (frame/s) rate. The signal frames are delivered to a 680 (MB/s) bandwidth camera link with frame transfers at 14 (bit/pixel) × 42.9 (Mpixel/s) = 75 MB/s, which require a storage of 4.3 TB over 16 (h).

A compute platform may scale-transform an 8-wavelength intensity vector per pixel spectral image with 24 floating point operations comprising 8 additions and 8 multiplies followed by 8 branch comparisons of a given library cell type. 10 cell libraries then require 10 × 24 (Flops/pixel) × 42.9 (Mpixel/s) = 10.3 (GFlops/s) capability. Commercially available edge computing coupled with other cloud resources can handle the computational complexity and storage required for processing large numbers of cell libraries in a secure and scalable manner.

C. Sample mechanical handling

A sample stage motion in an X-Y plane relative to optics aligned along a Z-axis illuminates a series of optical FOV's. Stage coordinates are generated via a linear encoder. After illumination across a band of wavelengths, the stage moves a sample to the next field location. Stage control is determined by photon flux requirements linked to dwell time per field, frame rate, and motion between fields. The latter may be set at ~20% of the dwell time to illuminate a single field with multiple wavelengths. For a 1.384 mm × 1.036 mm = 1.434 (mm^2) field imaged by the sensor array, the stage halts 267 ms for 8 exposures at 30 (frame/s). By accelerating 36 (mg) to reach 19 (mm/s) midway at 0.52 (mm), the stage then decelerates to the next image field in ~54 ms. A 300 (mm) diameter substrate

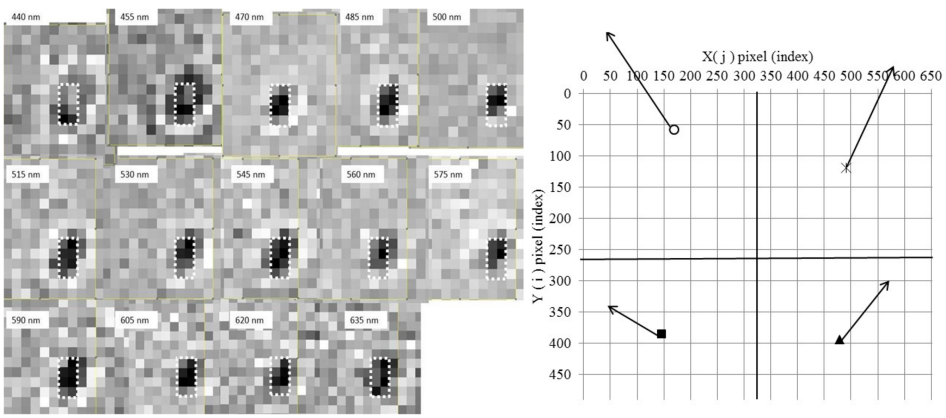

FIG. 5. (left) a series of monochromatic bright field images showing variable contrast at an RBC sample artifact calibration site (0.4 μm/pixel); (right) measured chromatic distortion at four sites.

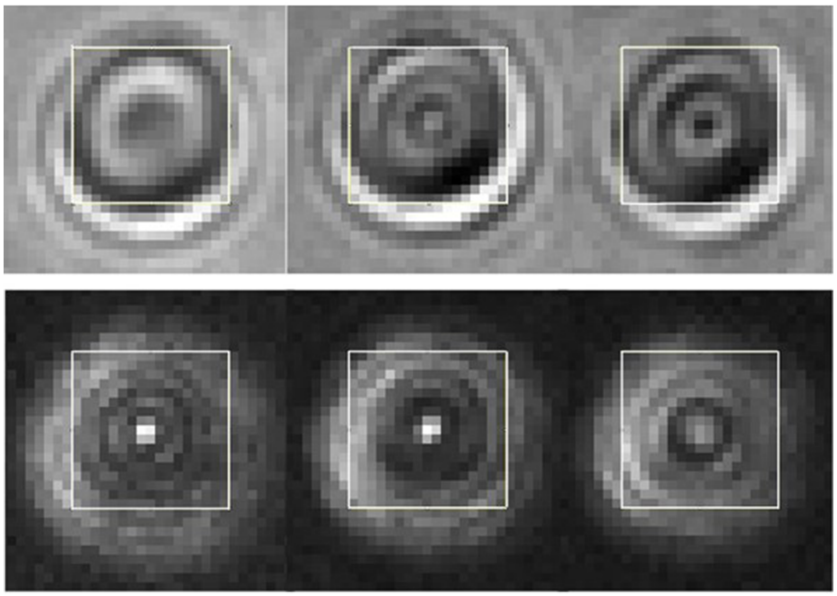

FIG. 6. The figure shows an image series of an erythrocyte (red blood cell): top row (bright field) and bottom row (dark field). Left to right: monochromatic images at wavelengths of 440, 530, and 620 (nm). Box length 17 pixels = 6.8 (μm).

covers 7.07×10^4 mm^2/1.45 mm^2 = 4.87×10^4 fields. As the total time per field is 321 (ms), the average rate 3.12 (fields/s) yields a 4.3-h throughput = 4.8×10^4 (fields)/3.12 (image-fields/s) with 1 μm pixels or 17.1 h with 0.5 μm pixels at the sample. Further throughput improvements are possible using a 4096 × 3000 CCD array (Sony IMX253) if a corresponding decrease in photo flux and signal to noise is acceptable. A throughput of 4.6 h can be achieved by adjusting magnification to M = 6.9, which transfers 0.5 μm sample pixels to the 3.45 (μm) CCD pixel, and increasing peak stage acceleration and velocity to 105 (mg) and 81 (m/s).

A variety of sample types can be measured given that a thin film is dispersed over an optically flat substrate, such as for a 0.7 ml blood sample spread over a 300-mm wafer with a ~10 μm film thickness. A reflective optics may use a semiconductor wafer or with transmission optics, a quartz blank or glass slide. Blood is a complex non-Newtonian fluid, but 1–100 (cPoise) viscosity is comparable to photoresist, and uniform thin film thickness may be achieved via a spray, spin coating, or microfluidic method.

D. Red blood cell spectral images

Spectral image microscopy reveals a variety of cell features. An unstained red blood cell (Rbc) shown in Fig. 6 at 0.4 (μm/pixel) superposes some partially coherent, phase object characteristics on the Gaussian image. The 10× objective lens with numerical aperture (NA) = 0.5 results in a resolution of ~0.44–0.54 (μm) at 440 (nm) wavelength for dark field apodization and bright field imaging, respectively.[14] The 6.8 (μm) Rbc cell diameter bounded by the box is estimated from the dark fringe boundary in the bright field image series (top row). The diffraction rings extend to ~11.2 (μm) diameter at 440 (nm). The biconcave red blood cell results in a bright contrast 2 × 2 pixel [0.8 (μm) square] central region, visible in the dark field series, in part, due to an order of magnitude greater molar extinction coefficient at 440 nm compared to 620 nm.[16] Partially coherent illumination by unscattered light emitted in a relatively narrow 6° emission semi-angle from the thin central region of the cell may explain the nature of the interference rings.[14]

III. CONCLUSION

A high throughput spectral image microscopy system can process a 1 (ml) aliquot blood sample of 5×10^9 cells in 5–17 h with 0.5 μm pixel resolution. Further improvements may be possible as limits to acceptable pixel size are explored. A separate paper will describe a classification algorithm applied to a variety of cells.

ACKNOWLEDGMENTS

The authors wish to thank our colleagues for useful discussions on optics: Tim Thomas, Doug Holmgren, and Zach Smith, and bio-medical applications: Robert Goldsby and Stephen Lane. This work was partially supported by the Center for Biophotonics Science and Technology, a designated National Science Foundation Science and Technology Center managed by the University of California Davis under Cooperative Agreement No. PHY0120999.

[1] L. Herzenberg, Kyoto Prize Lecture, 2006.
[2] L. M. Clover *et al.*, "A three-colour flow cytometry technique for measuring trophoblast intracellular antigens: The relative expression of TAP1 in human cytotrophoblast and decidual cells," Placenta **21**, 743–753 (2000).
[3] D. Peters *et al.*, "The LLNL high-speed sorter: Design features, operational characteristics, and biological utility," Cytometry **6**, 290–301 (1985).
[4] H. Steen, "Noise, sensitivity, and resolution of flow cytometers," Cytometry **13**, 822–830 (1992).
[5] D. Heller, "A review and applications of flow cytometry," https://www.scribd.com/ (2004).
[6] H. Hsieh *et al.*, "High speed detection of circulating tumor cells," Biosens. Bioelectron. **21**, 1893–1899 (2006).
[7] J. Chan*et al.*, "Reagentless identification of single bacterial spores in aqueous solution by confocal laser tweezers Raman spectroscopy," Anal. Chem. **76**, 599–603 (2004); Micro-Raman spectroscopy detects individual

neoplastic and normal hematopoietic cells," Biophys. J. **90**, 648–656 (2006).
[8]Z. Malik *et al.*, "Spectral morphometric characterization of B-CLL cells versus normal small lymphocytes," J. Histochem. Cytochem. **46**(10), 1113–1118 (1998).
[9]N. Katzilakis *et al.*, "Spectral characteristics of acute lymphoblastic leukemia in childhood," Leuk. Res. **28**(11), 1159–1164 (2004).
[10]C. Greiner *et al.*, "Confocal backscattering spectroscopy for leukemic and normal blood cell discrimination," Cytometry, Part A **79A**, 866–873 (2011).
[11]I. Itzkan *et al.*, "Confocal light absorption and scattering spectroscopic microscopy monitors organelles in live cells with no exogenous labels," Proc. Natl. Acad. Sci. U. S. A. **104**(44), 17255–17260 (2007).
[12]K.-H. Lim *et al.*, "Light-scattering spectroscopy differentiates fetal from adult nucleated red blood cells: May lead to noninvasive prenatal diagnosi," Opt. Lett. **34**(9), 1483–1485 (2009).
[13]M. Gesley, "Pattern generation," in *Photomask Fabrication Technology*, edited by W. Eynon (McGraw-Hill 2005) Chap. 3; M. Gesley, "A system for image rendering or spectral recognition," U.S. Patent 8,913,121 B2 (16 December 2014).
[14]M. Born and E. Wolf, *Principles of Optics*, 7th ed. (Cambridge University Press, 1999), Vol. 472, p. 598.
[15]R. Alfano, *The Supercontinuum Laser Source: Fundamentals with Updated References* (Springer, 2006).
[16]S. Prahl, "Optical Absorption of Hemoglobin," http://omlc.org/spectra/hemoglobin/index.html.